Measurement of $\Delta^{++}(1232)$ production in hadronic Z decays

DELPHI Collaboration

P. Abreu[u], W. Adam[ay], T. Adye[ak], E. Agasi[ae], I. Ajinenko[ap], R. Aleksan[am], G.D. Alekseev[p], P.P. Allport[v], S. Almehed[x], S.J. Alvsvaag[d], U. Amaldi[i], S. Amato[au], A. Andreazza[ab], M.L. Andrieux[n], P. Antilogus[i], V. Anykeyev[ap], W-D. Apel[q], Y. Arnoud[am], B. Åsman[ar], J-E. Augustin[s], A. Augustinus[ae], P. Baillon[i], P. Bambade[s], F. Barao[u], R. Barate[n], D.Y. Bardin[p], G.J. Barker[ai], A. Baroncelli[an], O. Barring[x], J.A. Barrio[z], W. Bartl[ay], M.J. Bates[ak], M. Battaglia[o], M. Baubillier[w], J. Baudot[am], K-H. Becks[ba], M. Begalli[f], P. Beilliere[h], Yu. Belokopytov[i], A.C. Benvenuti[e], M. Berggren[au], D. Bertrand[b], F. Bianchi[as], M. Bigi[as], M.S. Bilenky[p], P. Billoir[w], D. Bloch[j], M. Blume[ba], S. Blyth[ai], V. Bocci[aℓ], T. Bolognese[am], M. Bonesini[ab], W. Bonivento[ab], P.S.L. Booth[v], G. Borisov[ap], C. Bosio[an], S. Bosworth[ai], O. Botner[av], B. Bouquet[s], C. Bourdarios[i], T.J.V. Bowcock[v], M. Bozzo[m], P. Branchini[an], K.D. Brand[aj], T. Brenke[ba], R.A. Brenner[o], C. Bricman[b], L. Brillault[w], R.C.A. Brown[i], P. Bruckman[r], J-M. Brunet[h], L. Bugge[ag], T. Buran[ag], T. Burgsmueller[ba], P. Buschmann[ba], A. Buys[i], M. Caccia[ab], M. Calvi[ab], A.J. Camacho Rozas[ao], T. Camporesi[i], V. Canale[aℓ], M. Canepa[m], K. Cankocak[ar], F. Cao[b], F. Carena[i], P. Carrilho[au], L. Carroll[v], C. Caso[m], M.V. Castillo Gimenez[aw], A. Cattai[i], F.R. Cavallo[e], L. Cerrito[aℓ], V. Chabaud[i], Ph. Charpentier[i], L. Chaussard[y], J. Chauveau[w], P. Checchia[aj], G.A. Chelkov[p], R. Chierici[as], P. Chliapnikov[ap], P. Chochula[g], V. Chorowicz[i], V. Cindro[aq], P. Collins[i], J.L. Contreras[s], R. Contri[m], E. Cortina[aw], G. Cosme[s], F. Cossutti[at], H.B. Crawley[a], D. Crennell[ak], G. Crosetti[m], J. Cuevas Maestro[ah], S. Czellar[o], E. Dahl-Jensen[ac], J. Dahm[ba], B. Dalmagne[s], M. Dam[ag], G. Damgaard[ac], A. Daum[q], P.D. Dauncey[ak], M. Davenport[i], W. Da Silva[w], C. Defoix[h], G. Della Ricca[at], P. Delpierre[aa], N. Demaria[ai], A. De Angelis[i], H. De Boeck[b], W. De Boer[q], S. De Brabandere[b], C. De Clercq[b], C. De La Vaissiere[w], B. De Lotto[at], A. De Min[ab], L. De Paula[au], C. De Saint-Jean[am], H. Dijkstra[i], L. Di Ciaccio[aℓ], F. Djama[j], J. Dolbeau[h], M. Donszelmann[i], K. Doroba[az], M. Dracos[j], J. Drees[ba], K.-A. Drees[ba], M. Dris[af], Y. Dufour[h], F. Dupont[n], D. Edsall[a], R. Ehret[q], G. Eigen[d], T. Ekelof[av], G. Ekspong[ar], M. Elsing[ba], J-P. Engel[j], N. Ershaidat[w], B. Erzen[aq], M. Espirito Santo[u], E. Falk[x], D. Fassouliotis[af], M. Feindt[i], A. Ferrer[aw], T.A. Filippas[af], A. Firestone[a], P.-A. Fischer[j], H. Foeth[i], E. Fokitis[af], F. Fontanelli[m], F. Formenti[i], B. Franek[ak], P. Frenkiel[h], D.C. Fries[q], A.G. Frodesen[d], R. Fruhwirth[ay],

F. Fulda-Quenzer[s], J. Fuster[aw], A. Galloni[v], D. Gamba[as], M. Gandelman[f], C. Garcia[aw],
J. Garcia[ao], C. Gaspar[i], U. Gasparini[aj], Ph. Gavillet[i], E.N. Gazis[af], D. Gele[j], J-P. Gerber[j],
M. Gibbs[v], R. Gokieli[az], B. Golob[aq], G. Gopal[ak], L. Gorn[a], M. Gorski[az], Yu. Gouz[ap],
V. Gracco[m], E. Graziani[an], G. Grosdidier[s], P. Gunnarsson[ar], M. Gunther[av], J. Guy[ak],
U. Haedinger[q], F. Hahn[i], M. Hahn[q], S. Hahn[ba], Z. Hajduk[r], A. Hallgren[av],
K. Hamacher[ba], W. Hao[ae], F.J. Harris[ai], V. Hedberg[x], R. Henriques[u], J.J. Hernandez[aw],
P. Herquet[b], H. Herr[i], T.L. Hessing[i], E. Higon[aw], H.J. Hilke[i], T.S. Hill[a], S-O. Holmgren[ar],
P.J. Holt[ai], D. Holthuizen[ae], M. Houlden[v], J. Hrubec[ay], K. Huet[b], K. Hultqvist[ar],
P. Ioannou[c], J.N. Jackson[v], R. Jacobsson[ar], P. Jalocha[r], R. Janik[g], G. Jarlskog[x], P. Jarry[am],
B. Jean-Marie[s], E.K. Johansson[ar], L. Jonsson[x], P. Jonsson[x], C. Joram[i], P. Juillot[j],
M. Kaiser[q], F. Kapusta[w], M. Karlsson[ar], E. Karvelas[k], S. Katsanevas[c], E.C. Katsoufis[af],
R. Keranen[o], B.A. Khomenko[p], N.N. Khovanski[p], B. King[v], N.J. Kjaer[ac], H. Klein[i],
A. Klovning[d], P. Kluit[ae], J.H. Koehne[q], B. Koene[ae], P. Kokkinias[k], M. Koratzinos[i],
V. Kostioukhine[ap], C. Kourkoumelis[c], O. Kouznetsov[m], P.-H. Kramer[ba], M. Krammer[ay],
C. Kreuter[q], J. Krolikowski[az], I. Kronkvist[x], Z. Krumstein[p], W. Krupinski[r], P. Kubinec[g],
W. Kucewicz[r], K. Kurvinen[o], C. Lacasta[aw], I. Laktineh[y], S. Lamblot[w], J.W. Lamsa[a],
L. Lanceri[at], D.W. Lane[a], P. Langefeld[ba], V. Lapin[ap], I. Last[v], J-P. Laugier[am],
R. Lauhakangas[o], G. Leder[ay], F. Ledroit[n], V. Lefebure[b], C.K. Legan[a], R. Leitner[ad],
Y. Lemoigne[am], J. Lemonne[b], G. Lenzen[ba], V. Lepeltier[s], T. Lesiak[aj], D. Liko[ay],
R. Lindner[ba], A. Lipniacka[s], I. Lippi[aj], B. Loerstad[x], M. Lokajicek[ℓ], J.G. Loken[ai],
J.M. Lopez[ao], A. Lopez-Fernandez[i], M.A. Lopez Aguera[ao], D. Loukas[k], P. Lutz[am],
L. Lyons[ai], G. Maehlum[q], A. Maio[u], V. Malychev[p], F. Mandl[ay], J. Marco[ao],
B. Marechal[au], M. Margoni[aj], J-C. Marin[i], C. Mariotti[an], A. Markou[k], T. Maron[ba],
C. Martinez-Rivero[ao], F. Martinez-Vidal[aw], S. Marti i Garcia[aw], F. Matorras[ao],
C. Matteuzzi[ab], G. Matthiae[aℓ], M. Mazzucato[aj], M. Mc Cubbin[i], R. Mc Kay[a],
R. Mc Nulty[v], J. Medbo[av], C. Meroni[ab], W.T. Meyer[a], M. Michelotto[aj], E. Migliore[as],
L. Mirabito[y], W.A. Mitaroff[ay], U. Mjoernmark[x], T. Moa[ar], R. Moeller[ac], K. Moenig[i],
M.R. Monge[m], P. Morettini[m], H. Mueller[q], L.M. Mundim[f], W.J. Murray[ak], B. Muryn[r],
G. Myatt[ai], F. Naraghi[n], F.L. Navarria[e], S. Navas[aw], P. Negri[ab], S. Nemecek[ℓ],
W. Neumann[ba], N. Neumeister[ay], R. Nicolaidou[c], B.S. Nielsen[ac], M. Nieuwenhuizen[ae],
V. Nikolaenko[j], P. Niss[ar], A. Nomerotski[aj], A. Normand[ai], W. Oberschulte-Beckmann[q],
V. Obraztsov[ap], A.G. Olshevski[p], A. Onofre[u], R. Orava[o], K. Osterberg[o], A. Ouraou[am],
P. Paganini[s], M. Paganoni[i], P. Pages[j], H. Palka[r], Th.D. Papadopoulou[af], L. Pape[i],
C. Parkes[ai], F. Parodi[m], A. Passeri[an], M. Pegoraro[aj], H. Pernegger[ay], M. Pernicka[ay],
A. Perrotta[e], C. Petridou[at], A. Petrolini[m], H.T. Phillips[ak], G. Piana[m], F. Pierre[am],
M. Pimenta[u], M. Pindo[ab], S. Plaszczynski[s], O. Podobrin[q], M.E. Pol[f], G. Polok[r],
P. Poropat[at], V. Pozdniakov[p], M. Prest[at], P. Privitera[aℓ], N. Pukhaeva[p], A. Pullia[ab],
D. Radojicic[ai], S. Ragazzi[ab], H. Rahmani[af], J. Rames[ℓ], P.N. Ratoff[t], A.L. Read[ag],
M. Reale[ba], P. Rebecchi[s], N.G. Redaelli[ab], M. Regler[ay], D. Reid[i], P.B. Renton[ai],
L.K. Resvanis[c], F. Richard[s], J. Richardson[v], J. Ridky[ℓ], G. Rinaudo[as], I. Ripp[am],

A. Romero[as], I. Roncagliolo[m], P. Ronchese[aj], L. Roos[n], E.I. Rosenberg[a], E. Rosso[i],
P. Roudeau[s], T. Rovelli[e], W. Ruckstuhl[ae], V. Ruhlmann-Kleider[am], A. Ruiz[ao], K. Rybicki[r],
A. Rybin[ap], H. Saarikko[o], Y. Sacquin[am], A. Sadovsky[p], G. Sajot[n], J. Salt[aw], J. Sanchez[z],
M. Sannino[m], H. Schneider[q], M.A.E. Schyns[ba], G. Sciolla[as], F. Scuri[at], P. Seager[t],
Y. Sedykh[p], A.M. Segar[ai], A. Seitz[q], R. Sekulin[ak], R.C. Shellard[f], I. Siccama[ae],
P. Siegrist[am], S. Simonetti[am], F. Simonetto[aj], A.N. Sisakian[p], B. Sitar[g], T.B. Skaali[ag],
G. Smadja[y], O. Smirnova[p], G.R. Smith[ak], R. Sosnowski[az], D. Souza-Santos[f], T. Spassov[u],
E. Spiriti[an], P. Sponholz[ba], S. Squarcia[m], C. Stanescu[an], S. Stapnes[ag], I. Stavitski[aj],
K. Stepaniak[az], F. Stichelbaut[i], A. Stocchi[s], J. Strauss[ay], R. Strub[j], B. Stugu[d],
M. Szczekowski[az], M. Szeptycka[az], T. Tabarelli[ab], J.P. Tavernet[w], O. Tchikilev[ap],
A. Tilquin[aa], J. Timmermans[ae], L.G. Tkatchev[p], T. Todorov[j], D.Z. Toet[ae], A. Tomaradze[b],
B. Tome[u], L. Tortora[an], G. Transtromer[x], D. Treille[i], W. Trischuk[i], G. Tristram[h],
A. Trombini[s], C. Troncon[ab], A. Tsirou[i], M-L. Turluer[am], I.A. Tyapkin[p], M. Tyndel[ak],
S. Tzamarias[v], B. Ueberschaer[ba], O. Ullaland[i], V. Uvarov[ap], G. Valenti[e], E. Vallazza[i],
C. Vander Velde[b], G.W. Van Apeldoorn[ae], P. Van Dam[ae], W.K. Van Doninck[b],
J. Van Eldik[ae], N. Vassilopoulos[ai], G. Vegni[ab], L. Ventura[aj], W. Venus[ak], F. Verbeure[b],
M. Verlato[aj], L.S. Vertogradov[p], D. Vilanova[am], P. Vincent[y], L. Vitale[at], E. Vlasov[ap],
A.S. Vodopyanov[p], V. Vrba[ℓ], H. Wahlen[ba], C. Walck[ar], F. Waldner[at], M. Weierstall[ba],
P. Weilhammer[i], A.M. Wetherell[i], D. Wicke[ba], J.H. Wickens[b], M. Wielers[q],
G.R. Wilkinson[ai], W.S.C. Williams[ai], M. Winter[j], M. Witek[i], K. Woschnagg[av], K. Yip[ai],
O. Yushchenko[ap], F. Zach[y], C. Zacharatou[x], A. Zaitsev[ap], A. Zalewska[r], P. Zalewski[az],
D. Zavrtanik[aq], E. Zevgolatakos[k], V. Zhigunov[ap], N.I. Zimin[p], M. Zito[am], D. Zontar[aq],
R. Zuberi[ai], G.C. Zucchelli[ar], G. Zumerle[aj]

[a] Ames Laboratory and Department of Physics, Iowa State University, Ames IA 50011, USA
[b] Physics Department, Univ. Instelling Antwerpen, Universiteitsplein 1, B-2610 Wilrijk, Belgium
and IIHE, ULB-VUB, Pleinlaan 2, B-1050 Brussels, Belgium
and Faculté des Sciences, Univ. de l'Etat Mons, Av. Maistriau 19, B-7000 Mons, Belgium
[c] Physics Laboratory, University of Athens, Solonos Str. 104, GR-10680 Athens, Greece
[d] Department of Physics, University of Bergen, Allégaten 55, N-5007 Bergen, Norway
[e] Dipartimento di Fisica, Università di Bologna and INFN, Via Irnerio 46, I-40126 Bologna, Italy
[f] Centro Brasileiro de Pesquisas Físicas, rua Xavier Sigaud 150, RJ-22290 Rio de Janeiro, Brazil
and Depto. de Física, Pont. Univ. Católica, C.P. 38071 RJ-22453 Rio de Janeiro, Brazil
and Inst. de Física, Univ. Estadual do Rio de Janeiro, rua São Francisco Xavier 524, Rio de Janeiro, Brazil
[g] Comenius University, Faculty of Mathematics and Physics, Mlynska Dolina, SK-84215 Bratislava, Slovakia
[h] Collège de France, Lab. de Physique Corpusculaire, IN2P3-CNRS, F-75231 Paris Cedex 05, France
[i] CERN, CH-1211 Geneva 23, Switzerland
[j] Centre de Recherche Nucléaire, IN2P3 - CNRS/ULP - BP20, F-67037 Strasbourg Cedex, France
[k] Institute of Nuclear Physics, N.C.S.R. Demokritos, P.O. Box 60228, GR-15310 Athens, Greece
[ℓ] FZU, Inst. of Physics of the C.A.S. High Energy Physics Division, Na Slovance 2, 180 40, Praha 8, Czech Republic
[m] Dipartimento di Fisica, Università di Genova and INFN, Via Dodecaneso 33, I-16146 Genova, Italy
[n] Institut des Sciences Nucléaires, IN2P3-CNRS, Université de Grenoble 1, F-38026 Grenoble Cedex, France
[o] Research Institute for High Energy Physics, SEFT, P.O. Box 9, FIN-00014 Helsinki, Finland
[p] Joint Institute for Nuclear Research, Dubna, Head Post Office, P.O. Box 79, 101 000 Moscow, Russian Federation
[q] Institut für Experimentelle Kernphysik, Universität Karlsruhe, Postfach 6980, D-76128 Karlsruhe, Germany
[r] High Energy Physics Laboratory, Institute of Nuclear Physics, Ul. Kawiory 26a, PL-30055 Krakow 30, Poland
[s] Université de Paris-Sud, Lab. de l'Accélérateur Linéaire, IN2P3-CNRS, Bât. 200, F-91405 Orsay Cedex, France
[t] School of Physics and Materials, University of Lancaster, Lancaster LA1 4YB, UK

[u] LIP, IST, FCUL - Av. Elias Garcia, 14-1(o), P-1000 Lisboa Codex, Portugal

[v] Department of Physics, University of Liverpool, P.O. Box 147, Liverpool L69 3BX, UK

[w] LPNHE, IN2P3-CNRS, Universités Paris VI et VII, Tour 33 (RdC), 4 place Jussieu, F-75252 Paris Cedex 05, France

[x] Department of Physics, University of Lund, Sölvegatan 14, S-22363 Lund, Sweden

[y] Université Claude Bernard de Lyon, IPNL, IN2P3-CNRS, F-69622 Villeurbanne Cedex, France

[z] Universidad Complutense, Avda. Complutense s/n, E-28040 Madrid, Spain

[aa] Univ. d'Aix - Marseille II - CPP, IN2P3-CNRS, F-13288 Marseille Cedex 09, France

[ab] Dipartimento di Fisica, Università di Milano and INFN, Via Celoria 16, I-20133 Milan, Italy

[ac] Niels Bohr Institute, Blegdamsvej 17, DK-2100 Copenhagen 0, Denmark

[ad] NC, Nuclear Centre of MFF, Charles University, Areal MFF, V Holesovickach 2, 180 00, Praha 8, Czech Republic

[ae] NIKHEF-H, Postbus 41882, NL-1009 DB Amsterdam, The Netherlands

[af] National Technical University, Physics Department, Zografou Campus, GR-15773 Athens, Greece

[ag] Physics Department, University of Oslo, Blindern, N-1000 Oslo 3, Norway

[ah] Dpto. Fisica, Univ. Oviedo, C/P. Pérez Casas, S/N-33006 Oviedo, Spain

[ai] Department of Physics, University of Oxford, Keble Road, Oxford OX1 3RH, UK

[aj] Dipartimento di Fisica, Università di Padova and INFN, Via Marzolo 8, I-35131 Padua, Italy

[ak] Rutherford Appleton Laboratory, Chilton, Didcot OX11 OQX, UK

[al] Dipartimento di Fisica, Università di Roma II and INFN, Tor Vergata, I-00173 Rome, Italy

[am] Centre d'Etudes de Saclay, DSM/DAPNIA, F-91191 Gif-sur-Yvette Cedex, France

[an] Istituto Superiore di Sanità, Ist. Naz. di Fisica Nucl. (INFN), Viale Regina Elena 299, I-00161 Rome, Italy

[ao] C.E.A.F.M., C.S.I.C. - Univ. Cantabria, Avda. los Castros, (CICYT-AEN93-0832), S/N-39006 Santander, Spain

[ap] Inst. for High Energy Physics, Serpukov P.O. Box 35, Protvino, (Moscow Region), Russian Federation

[aq] J. Stefan Institute and Department of Physics, University of Ljubljana, Jamova 39, SI-61000 Ljubljana, Slovenia

[ar] Fysikum, Stockholm University, Box 6730, S-113 85 Stockholm, Sweden

[as] Dipartimento di Fisica Sperimentale, Università di Torino and INFN, Via P. Giuria 1, I-10125 Turin, Italy

[at] Dipartimento di Fisica, Università di Trieste and INFN, Via A. Valerio 2, I-34127 Trieste, Italy
and Istituto di Fisica, Università di Udine, I-33100 Udine, Italy

[au] Univ. Federal do Rio de Janeiro, C.P. 68528 Cidade Univ., Ilha do Fundão BR-21945-970 Rio de Janeiro, Brazil

[av] Department of Radiation Sciences, University of Uppsala, P.O. Box 535, S-751 21 Uppsala, Sweden

[aw] IFIC, Valencia-CSIC, and D.F.A.M.N., U. de Valencia, Avda. Dr. Moliner 50, E-46100 Burjassot (Valencia), Spain

[ay] Institut für Hochenergiephysik, Österr. Akad. d. Wissensch., Nikolsdorfergasse 18, A-1050 Vienna, Austria

[az] Inst. Nuclear Studies and University of Warsaw, Ul. Hoza 69, PL-00681 Warsaw, Poland

[ba] Fachbereich Physik, University of Wuppertal, Postfach 100 127, D-42097 Wuppertal 1, Germany

Abstract

A measurement of the Δ^{++}(1232) inclusive production in hadronic decays of the Z at LEP is presented, based on 1.3 million hadronic events collected by the DELPHI detector in the 1994 LEP running period. The DELPHI ring imaging Cherenkov counters are used for identifying hadrons. The average Δ^{++}(1232) multiplicity per hadronic event is 0.079 ± 0.015 which is more than a factor of two below the JETSET, HERWIG and UCLA model predictions. It agrees with a recently proposed universal mass dependence of particle production rates in e^+e^- annihilations.

1. Introduction

The LEP experiments have presented analyses of the inclusive production of various baryons [1] belonging to the SU(3) octet and decuplet, including protons [1–3], Λ [4–6,8–10], $\Sigma^{\pm,0}$ [6,7], Ξ^- [5,6,8,9], $\Sigma^{\pm}$(1385) [6,8,9], Ξ^0(1530) [6,8,9] Ω^- [7–9] and corresponding antibaryons.

The detection of Δ^{++}(1232) in the $p\pi^+$ invariant mass spectrum is difficult because it is a broad resonance with mass close to the peak in the phase space of $p\pi^+$ pairs and because of the large combinatorial

---

[1] Unless otherwise stated, antiparticles are implicitly included.

background. Therefore proton (antiproton) identification is essential for $\Delta^{++}(1232)$ detection. Even at lower energies, where the combinatorial background is smaller, the $\Delta^{++}(1232)$ production rate in e^+e^- annihilation has been measured only by ARGUS [11] at 10 GeV and an upper limit has been given by TASSO [12] at 35 GeV. OPAL [13] has recently published results on the $\Delta^{++}(1232)$ production from Z decays.

In this paper, results on $\Delta^{++}(1232)$ inclusive production at LEP are presented. The data were collected by the DELPHI experiment in 1994 at centre of mass energies around the Z pole, and correspond to about 1.3 million hadronic decays in total. The DELPHI Ring Imaging Cherenkov (RICH) detectors were fully operational allowing particle identification.

After a brief description of the DELPHI detector and the selection of hadronic Z decays, the charged particle identification procedure and the fitting procedure used for extraction of the $\Delta^{++}(1232)$ signal from the $p\pi^+$ invariant mass distribution are described. The $\Delta^{++}(1232)$ average multiplicity and its differential cross section are presented and compared with the expectations of the JETSET 7.4 PS [14,15], HERWIG 5.8 [16,17] and UCLA 7.44 [18] models and with the regularities in particle yields observed in Ref. [19].

2. Experimental procedure

2.1. Event and particle selection

A detailed description of the DELPHI detector can be found in Refs. [20,21]. Here, only the specific properties relevant to the present analysis are summarized.

The charged particle tracks are measured in the 1.2 T magnetic field by a set of tracking detectors. The average momentum resolution for charged particles in hadronic final states is in the range $\Delta p/p \simeq 0.001p$ to $0.01p$ (p in GeV/c), depending on which detectors are included in the track fit.

A charged particle is required to satisfy the following criteria: momentum greater than 0.2 GeV/c; $\Delta p < p$; polar angle θ with respect to the beam axis between 25° and 155°; measured track length in the Time Projection Chamber (TPC) greater than 50 cm and impact parameter with respect to the nominal crossing point within 5 cm in the transverse (xy) plane and 10

cm along the beam direction (z-axis).

Hadronic events are then selected if there are at least 5 charged particles, if the total energy of charged particles (assumed to be pions) in each of two hemispheres (θ above and below 90°) exceeds 3 GeV, if the total energy of all charged particles is greater than 15 GeV, if the polar angle of the sphericity axis is between 40° and 140° and if the information from the RICH detectors is available for at least one charged particle. The contamination from events due to beam-gas scattering and to $\gamma\gamma$ interactions is estimated to be less than 0.1% of the accepted events.

The sample of 846,627 events selected with the above cuts will be referred to below as the one with the weak cuts. However, in order to ensure a better signal-to-background ratio for the $\Delta^{++}(1232)$ in the $p\pi^+$ invariant mass spectrum, stronger restrictions on the track impact parameters with respect to the nominal crossing point were imposed: within 0.3 cm in the transverse plane and 2 cm along the beam direction. The sample selected with these additional cuts amounts to 820,375 events and will be referred to below as the one with the strong cuts.

2.2. Particle identification

Particle identification in this analysis is mainly provided by the RICH detectors. They enable identification of protons over the momentum range $1.5 \leq p \leq 25$ GeV/c. The RICH relies on external tracking for the determination of the particle momentum and impact point. The Barrel RICH, which plays the most important role in particle identification in this study, due to imposed restrictions on the polar angle θ of the particles, is placed between the TPC, the main tracking device of DELPHI, and another tracking detector, the Outer Detector (OD). For the veto mode of the RICH, requiring a track segment in the OD removes particles which were scattered or lost due to an interaction in the RICH. It also improves the quality of the track extrapolation. This is specially important for the liquid radiator, where the center of the Cherenkov ring is given by the impact point of the track. Therefore, the track of the selected particle was required to be detected in the OD.

Above the emission threshold, the Cherenkov angle θ_c depends on the velocity β of the particle, via the relation $\cos\theta_c = 1/n\beta$, where n is the refractive

index of the radiator medium. The number of photons emitted is proportional to $\sin^2 \theta_c$. For a track of known momentum, the expected Cherenkov signal can be computed in the pion[2], K and p mass hypotheses. It is characterised by the value of Cherenkov angle, its width and the number of photoelectrons.

The particle identification is based on the comparison between the measured Cherenkov angle with that expected for each mass hypothesis. This is called the ring identification mode (for more details, see [21] and refs. therein). The raw photoelectron distributions were described as the sum of the expected Cherenkov signal and a flat unknown background and their probability to come from π, K and proton calculated. For particles below the Cherenkov threshold, $\beta < 1/n$, no light is emitted. This property is used in order to separate kaons and protons in the momentum range where these are below the threshold while lighter particles emit photons. This is called the veto identification mode.

For particles with momentum $p \leq 1.5$ GeV/c, the corresponding probabilities were also calculated using the measurement of the ionization, dE/dx, in the TPC. These probabilities were combined to give the likelihood that the particle was a π, K or a proton.

The aim of the tagging algorithms was to provide a mass tag for individual particles. The identification performance was evaluated by means of the detector simulation program DELSIM [21]. In DELSIM, about 1.8 million events were generated using the JET-SET program [15] with the DELPHI default parameters [21]. The particles were followed through the detector and the simulated digitizations obtained were processed with the same reconstruction programs as the experimental data. The fraction of protons, kaons and pions which satisfied the weak cuts on the charged particle selection and were selected as protons by the RICH and TPC measurements are presented as a function of their momentum in Fig. 1. This figure shows that the efficiency of the proton identification is rather momentum independent and about 35% on average. In order to check the compatibility of the proton identification efficiencies in simulation and data, protons from reconstructed Λ decays were used. It was found that around 99% of such protons satisfied the weak

charged particle selection criteria. The average ratio between the proton identification efficiencies in data and simulation was found to be $(90 \pm 3)\%$. The $\Delta^{++}(1232)$ cross section determined in this analysis was corrected for this difference taking into account its small dependence on proton momentum. The corresponding uncertainties, taken conservatively equal to $\pm 9\%$, were accounted for in the systematic errors for the $\Delta^{++}(1232)$ cross sections (see below). The fraction of pions identified as protons is smaller than 0.8% over the whole momentum range and much smaller at the lowest momenta (Fig. 1). The fraction of kaons identified as protons is largest for the momentum range between 4.5 and 8.5 GeV/c, where it amounts to about 20% on average, but drops significantly below 10% in other momentum intervals. Thus, applying the proton selection significantly reduces the combinatorial background under the $\Delta^{++}(1232)$, with relatively small loss of the signal. Only those particles satisfying the proton selection were used as protons in the calculation of the pπ^+ invariant mass. All other particles were assigned the pion mass.

It is necessary to stress that particle identification provided by the DELPHI detector is the most important element in the experimental procedure for $\Delta^{++}(1232)$ detection. It was explicitly checked using the procedure described below that without particle identification, the signal-to-background ratio for $x_p \geq 0.03$ ($x_p = p(\text{p}\pi^+)/p_{\text{beam}}$) drops from 0.040 to 0.0039 in the pπ^+ mass range from 1.14 to 1.32 GeV/c^2 so that no $\Delta^{++}(1232)$ detection would be possible.

2.3. Treatment of detector imperfection and fit procedure

Particle identification inefficiencies as well as other detector imperfections, such as limited geometrical acceptance, particle interactions in the detector material etc, and different kinematical cuts imposed for charged particles and event selections, were taken into account by applying the approach described in Ref. [22].

In the present analysis a vector, a, of parameters was used in the definition of the anticipated distribution function, $f(M, a)$, of the invariant mass M. This function was composed of two parts:

$$f^R(M, a) = a_1 W(M) \cdot BW(M, a_2, a_3), \qquad (1)$$

---

[2] The muon and pion masses are so close that they cannot be distinguished.
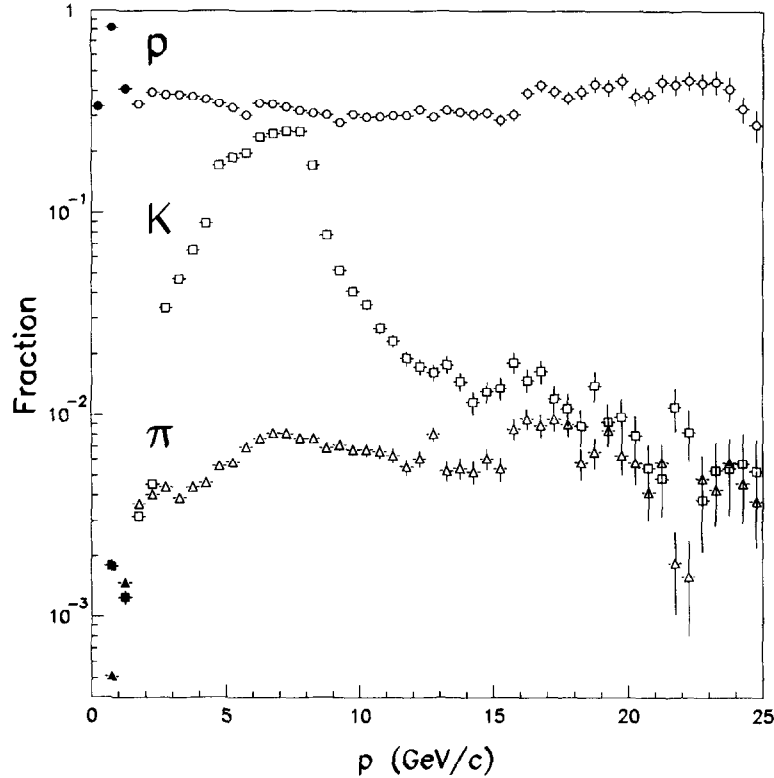
Fig. 1. The fractions of protons, kaons and pions as a function of their momentum generated in JETSET and identified as protons using the information from RICH (open symbols) and TPC (closed symbols) after full detector simulation.

describing the $\Delta^{++}(1232)$ resonance signal, and a background term:

$$f^B(M, a) = a_4(M - M_{th})^{a_5}$$
$$\cdot \exp(a_6 M + a_7 M^2 + a_8 M^3), \qquad (2)$$

where $BW(M, a_2, a_3)$ is a relativistic Breit–Wigner function:

$$BW(M, M_0, \Gamma_0) = \frac{M \cdot M_0 \cdot \Gamma(M)}{(M_0^2 - M^2)^2 + (M_0 \cdot \Gamma(M))^2},$$

$$\Gamma(M) = \Gamma_0 \cdot \left(\frac{q}{q_0}\right)^3 \cdot \frac{2q_0^2}{q_0^2 + q^2}.$$

Here q_0 and q are the momenta of the $\Delta^{++}(1232)$ decay products in the resonance c.m. system for masses M_0 and M, respectively, and M_{th} is the $p\pi^+$ invariant mass threshold.

The function $W(M)$ in Eq. (1), introduced in [22], accounts for distortion of the $\Delta^{++}(1232)$ Breit–

Wigner shape by phase space effects and by residual Bose–Einstein correlations. As in [22], it was obtained by generating the invariant mass distribution for the resonance using the JETSET program where Bose–Einstein correlations were included. Then the generated distribution (with its integral normalized to one) was divided by the analytical Breit–Wigner function used in JETSET (also normalized to one).

The function $W(M)$ was used in [22] to account for distortion of meson resonance (ρ^0 and $f_2(1270)$) Breit–Wigner shapes by residual Bose–Einstein correlations. For the $\Delta^{++}(1232)$, this distortion is expected to be smaller because only one particle coming from the decay can be affected by the Bose–Einstein effect. It was checked that the function $W(M)$ is almost independent of M when Bose–Einstein correlations are not included. Inclusion of correlations leads to a noticeable distortion of the $\Delta^{++}(1232)$ Breit–Wigner shape although it is smaller than in the case of the ρ^0. The effect is most important at the smallest x_p-values, as

expected [3].

In each mass bin, m, the number of entries predicted by the function $f(M, a)$ is given by

$$\bar{N}_m(a) = C_m \sum_n S_{mn} A_n f_n(a), \qquad (3)$$

where $f_n(a) = \int_{M_n}^{M_{n+1}} f(M, a) \, dM$ and M_n is the lower edge of n-th histogram bin of variable M. The vector A characterizes the detector acceptance and C the losses of particles due to selection criteria imposed and extra particles due to ghosts, secondary interactions etc. The smearing matrix S_{mn} is determined by the experimental resolution (see [22] for more details).

The best values for a were then determined by a least squares fit of the predictions of Eq. (3) to the measured values, N_m, in each bin by minimizing the function

$$\chi^2 = \sum_m (N_m - \bar{N}_m(a))^2 / \sigma_m^2$$
$$+ \sum_{i=2}^{i=3} (a_i - \bar{a}_i)^2 / (\Delta \bar{a}_i)^2, \qquad (4)$$

where $\sigma_m^2 = N_m + \sigma^2(\bar{N}_m)$ and $\sigma(\bar{N}_m) \ll \sqrt{N_m}$ is the error of $\bar{N}_m$ due to finite statistics of the simulation used to evaluate A, C and S_{mn}. The second sum in Eq. (4) constrains the $\Delta^{++}(1232)$ mass, $a_2 = M_0$, and width, $a_3 = \Gamma_0$, to the accepted values, $\bar{a}_2 = 1232 \pm 2$ MeV/c^2 and $\bar{a}_3 = 120 \pm 5$ MeV/c^2 [23].

Unfortunately Eq. (3) is not sufficient to describe the predictions in the situation where the contribution from the signal contains protons while that from the background is still strongly contaminated by particle pairs in which both particles may be pions or kaons. Here the coefficients, C_m, for the resonance signal and for the background are expected to be different. For this reason Eq. (3) was changed to

$$\bar{N}_m(a) = C_m^R \sum_n S_{mn}^R A_n^R f_n^R(a)$$
$$+ C_m^B \sum_n S_{mn}^B A_n^B f_n^B(a), \qquad (5)$$

[3] If the influence of phase space and residual Bose–Einstein correlations is ignored completely $(W(M) = 1)$, the measured $\Delta^{++}(1232)$ cross section decreases by 5%.

where the first and second terms are defined for the resonance signal and background, respectively.

The coefficients A, C and the smearing matrix S_{mn} are determined as before [22] but for the $p\pi^+$ sample, separately for the resonance signal and for the background, using the simulated data. The coefficients A and C are shown as a function of $p\pi^+$ invariant mass in Fig. 2 for the indicated intervals of the fractional momentum x_p. The coefficients A characterizing the detector acceptance exhibit only small dependence on $p\pi^+$ mass and they are almost the same for the $\Delta^{++}(1232)$ resonance signal and for the background, as expected. The coefficients C exhibit a smooth dependence on $M(p\pi^+)$, but are much larger for the background than for the resonance signal because of pion and kaon misidentification as the proton. As discussed earlier, the kaon misidentification is most significant in the momentum range from 4.5 to 8.5 GeV/c (Fig. 1). As a consequence, the largest difference between coefficients C for the resonance signal and for the background is observed in the x_p interval from 0.1 to 0.2. Thus the two separate terms in Eq. (5) responsible for the resonance signal and for the background are indeed necessary.

The "weak" event selection cuts, defined in Section 2.1, were chosen to ensure that the average charged particle multiplicity for the data and simulated events were the same. But due to imperfections of the simulation tuning, this is not necessarily the case if the strong cuts are applied. Indeed, the ratios of the $p\pi^+$ invariant mass distributions, $d\sigma/dM$, obtained for the samples with the weak and strong cuts are different for the data ($R_D = d\sigma_{weak}/d\sigma_{strong}$) and simulated events ($R_S$). To take this into account, the coefficients C were divided by the factor $R = R_D(M)/R_S(M)$ in each of the considered x_p-intervals. These factors were approximated by constants, since their dependence on M was small. The R value averaged over the full measured x_p-range equals 1.11 ± 0.04.

The $\Delta^{++}(1232)$ cross section was calculated as

$$\sigma(\Delta^{++}(1232)) = \int f^R(M, a) \, dM.$$

The reliability of the applied procedure has been verified with the simulated events. For this sample, the $p\pi^+$ invariant mass distributions in different x_p-intervals were fitted applying the formulae (1), (2), (4) and (5), but with the non-relativistic Breit–
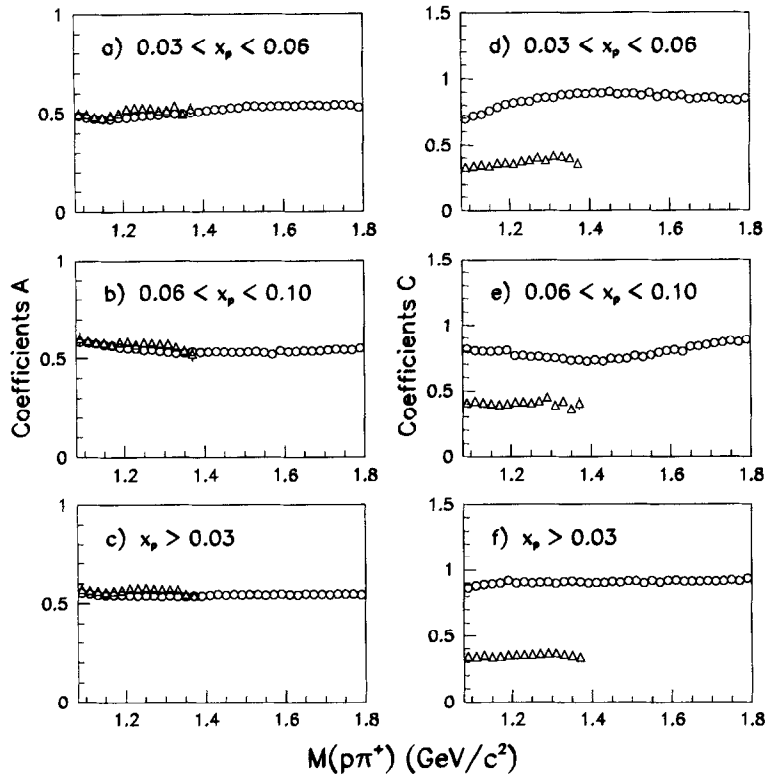
Fig. 2. The $p\pi^+$ invariant mass dependence of the coefficients A (a–c) and C (d–f) for the $\Delta^{++}(1232)$ resonance signal (triangles) and background (circles) for several x_p-intervals.

Wigner shape for the $\Delta^{++}(1232)$ used in JETSET. The results of such fits for several x_p-intervals are illustrated in Figs. 3a–3c. The fit describes the uncorrected simulated data very well. The $\Delta^{++}(1232)$ x_p-spectrum agrees within errors with that in JETSET. The "true" background (Eq. (2) with the parameters a found from these fits) is shown by the curves in Figs. 3d–3f in comparison with the background as generated by JETSET at the input to DELSIM (open points in Figs. 3d–3f). The agreement is also very good.

3. Results and discussion

The measured uncorrected $p\pi^+$ invariant mass distributions for the x_p intervals 0.03 to 0.06 and 0.06 to 0.10 (where $\Delta^{++}(1232)$ cross section gives the largest contribution to the overall measured cross section) and for the full measured $x_p \geq 0.03$ range are

shown in Figs. 4a to 4c, respectively together with the results of the fits. The fits describe the data very well. However, the $\Delta^{++}(1232)$ signal is smaller in the data (Figs. 4a to 4c) than in the simulated event sample (Figs. 3a to 3c), where JETSET with default parameters has been used. This shows that the $\Delta^{++}(1232)$ cross section in JETSET is grossly overestimated.

It is necessary to stress that the procedure applied for $\Delta^{++}(1232)$ detection is valid even in the case when the function $f(M, a)$ describing the true invariant mass distribution is quite different from the JETSET predictions, provided that the simulation adequately describes the detector imperfections and that the real background shape can indeed be parameterized by Eq. (2). Therefore, since the $\Delta^{++}(1232)$ signal is so small, additional tests were performed in order to check the stability of the result to changes in the conditions and background formulation, and to estimate the systematic uncertainties.

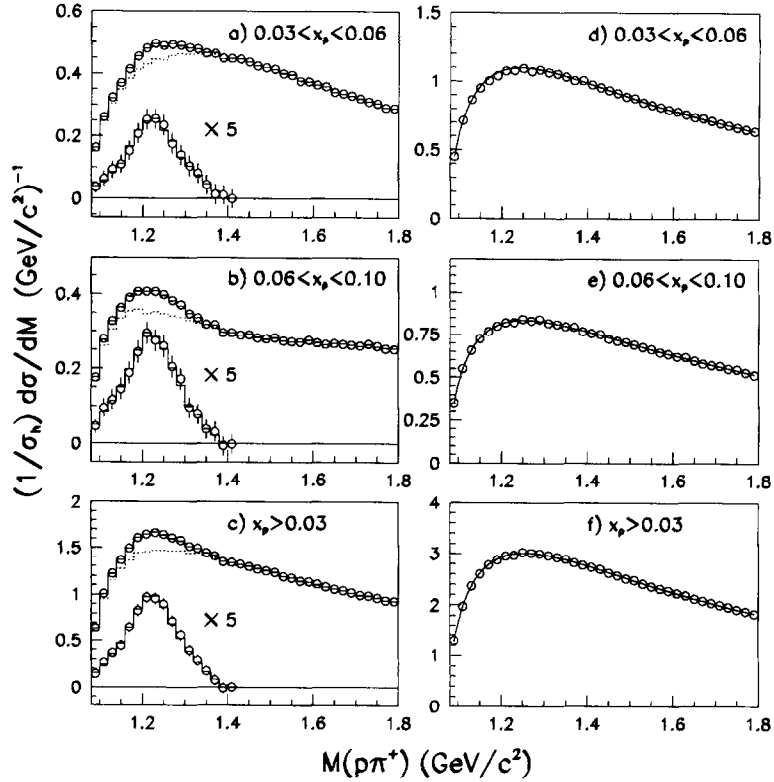A check was made to determine if the $p\pi^+$ mass

Fig. 3. (a–c): The $p\pi^+$ invariant mass spectra for indicated x_p-intervals for the uncorrected events after detector simulation (open points). The histograms are the results of the fit using the functions (1), (2), (4) and (5). The background is shown by the dashed histograms. The lower parts of the figures (with the amplification factor of 5) present the $\Delta^{++}(1232)$ signal and the results of the fit after background subtraction. (d–f): The $p\pi^+$ background as generated by JETSET (open points) in comparison with the function (2) with the parameters a found from the fits to the simulated data in Figs. a–c (full curves).

spectra can be satisfactorily fitted only by the background (2), without the $\Delta^{++}(1232)$ contribution. Such a fit over 36 bins of the $p\pi^+$ mass spectrum for $x_p \geq 0.03$ resulted in $\chi^2/\mathrm{NDF} = 101/31$ ($P(\chi^2) = 2 \cdot 10^{-9}$). Comparison with the corresponding fit probability $P(\chi^2) = 50\%$ ($\chi^2/\mathrm{NDF} = 29/30$) when the $\Delta^{++}(1232)$ contribution was included in the fit shows that the $\Delta^{++}(1232)$ signal is really present.

In order to test the sensitivity of the result to the background parameterization, a completely different form of the background was tried:

$$f^B(M', a) = a_4 \cdot (1 + a_5 M' + a_6 M'^2 + a_7 M'^{a_8})$$
$$\cdot BG(M'), \tag{6}$$

with $M' = (M - M_{th})/(M_{max} - M_{th})$ and $a_8 < 0$. The shape of this background was mainly determined by the function $BG(M')$, which was found using the

"mixed event" method, in which the proton was taken from one event and the π^+ from the subsequent one. The particle momenta were calculated in respect to the sphericity axes aligned in 3 dimensions. The function $1 + a_5 M' + a_6 M'^2 + a_7 M'^{a_8}$ took into account the imperfection of the mixed event method for the background estimate.

The $\Delta^{++}(1232)$ differential production cross section, $(1/\sigma_h) \cdot d\sigma/dx_p$, (where σ_h is the total hadronic cross section), obtained with these two different backgrounds (2) and (6), is presented in Table 1. The fits with the backgrounds (2) and (6) describe the data very well in all x_p intervals. The differential cross sections and the values of the average $\Delta^{++}(1232)$ multiplicity, $0.065 \pm 0.009(\mathrm{stat})$ and $0.072 \pm 0.008(\mathrm{stat})$, obtained with these two backgrounds, agree within errors. The result of the fit of the $p\pi^+$ invariant mass
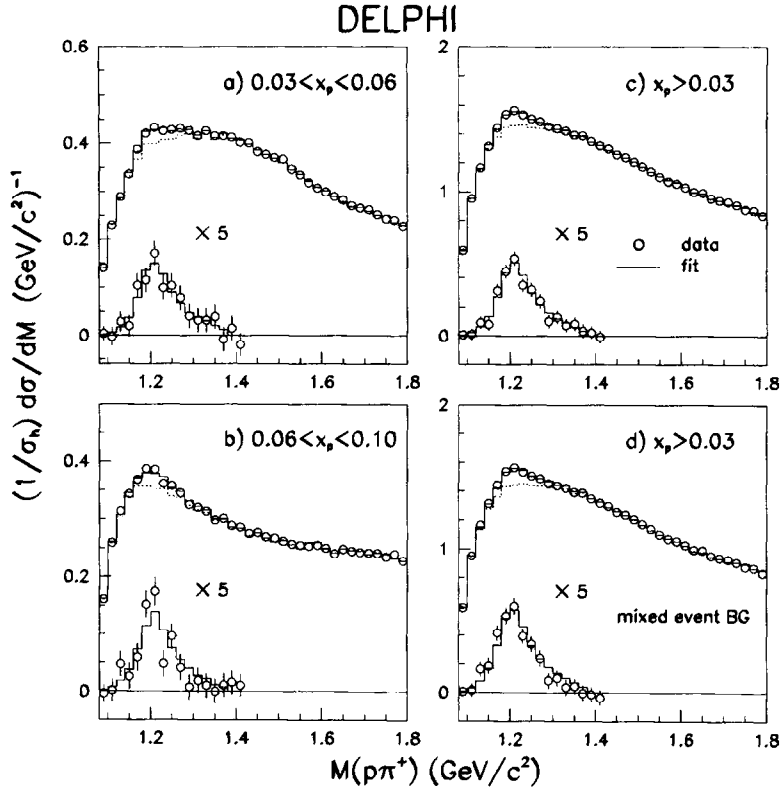
DELPHI

Fig. 4. The $p\pi^+$ invariant mass spectra for indicated x_p-intervals for the uncorrected data (open points). The histograms are the results of the fit using the functions (1), (2), (4) and (5) for Figs. 4a to 4c and (1), (4), (5) and (6) for Fig. 4d. The background is shown by the dashed histograms. The lower parts of the figures (with the amplification factor of 5) present the data and the results of the fit after background subtraction.

Table 1
Differential $\Delta^{++}(1232)$ cross sections $(1/\sigma_h)\cdot d\sigma/dx_p$ for $0.03 \leq x_p \leq 0.8$ obtained with the backgrounds (2) and (6). The errors are statistical. The corresponding values of χ^2/NDF for the fits are also given.

x_p-interval	Background (2)		Background (6)	
	$(1/\sigma_h)\cdot\frac{d\sigma}{dx_p}$	$\frac{\chi^2}{NDF}$	$(1/\sigma_h)\cdot\frac{d\sigma}{dx_p}$	$\frac{\chi^2}{NDF}$
0.03–0.06	0.76 ± 0.17	20/30	0.88 ± 0.14	25/30
0.06–0.10	0.38 ± 0.10	36/30	0.39 ± 0.08	35/30
0.1–0.2	0.14 ± 0.04	22/30	0.19 ± 0.04	24/30
0.2–0.4	0.06 ± 0.02	42/30	0.05 ± 0.02	36/30
0.4–0.8	0.004 ± 0.003	24/30	0.005 ± 0.002	21/30
0.03–0.8	0.065 ± 0.009	144/150	0.072 ± 0.008	141/150

distribution for $x_p \geq 0.03$ with the background (6) is shown for example in Fig. 4d.

The final measured average $\Delta^{++}(1232)$ multiplic-

ity per hadronic event for $x_p \geq 0.03$ was taken as the average of the values obtained with these two backgrounds:

$$< N(\Delta^{++}(1232) + \bar{\Delta}^{--}(1232)) >$$
$$= 0.069 \pm 0.008 \,(\text{stat}) + 0.008 \,(\text{syst}). \tag{7}$$

Half of the difference between these two values, amounting to 0.004 ($\pm 5\%$), was attributed to the systematic error in the background parameterization. The uncertainty in the coefficient R ($\pm 4\%$) accounting for an imperfection in the simulation and the uncertainty in the particle identification ($\pm 9\%$) were also accounted for in the overall systematic error in (7).

In a final test, the $\Delta^{++}(1232)$ cross section was determined using the same procedure as before (by averaging the results obtained with the two different backgrounds (2) and (6)), but in four different $\cos\theta_h$-intervals, where θ_h is the helicity angle of the
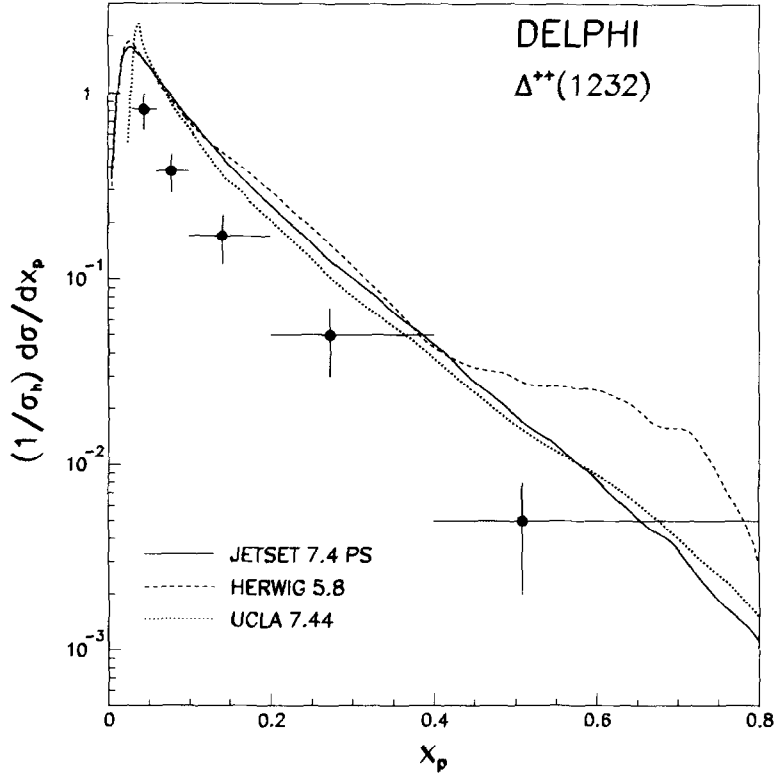
Fig. 5. Differential cross section $(1/\sigma_h) \cdot d\sigma/dx_p$ for inclusive $\Delta^{++}(1232)$ production. The statistical and systematic errors are combined quadratically. Full, dashed and dotted curves represent the expectations of JETSET 7.4 PS, HERWIG 5.8 and UCLA 7.44 models respectively with default parameters.

proton in the $p\pi^+$ rest frame with respect to the $p\pi^+$ line of flight. The $\cos\theta_h$ distribution is expected to be flat (in absence of $\Delta^{++}(1232)$ spin alignment) or at least symmetric around $\cos\theta_h = 0$. It therefore represents a good test of the assumed parameterization of the background, especially because the shape of the background is quite different in the different $\cos\theta_h$-intervals. The $\Delta^{++}(1232)$ differential cross section, $(1/\sigma_h) \cdot d\sigma/d\cos\theta_h$, obtained in the $0.03 \leq x_p \leq 0.8$ range is presented in Table 2. One can see that it is indeed flat within errors. The $\Delta^{++}(1232)$ average multiplicity obtained by summing over the $\cos\theta_h$-bins amounted to 0.066 ± 0.011 (tot). It is in good agreement with the value (7).

Table 2 and Fig. 5 also show the final $\Delta^{++}(1232)$ differential production cross section, $(1/\sigma_h) \cdot d\sigma/dx_p$, obtained in a similar way (by averaging the results obtained with the two different backgrounds (2) and (6)). In Fig. 5 the $\Delta^{++}(1232)$ differential cross sec-

Table 2
Differential $\Delta^{++}(1232)$ cross sections $(1/\sigma_h) \cdot d\sigma/dx_p$ and $(1/\sigma_h) \cdot d\sigma/d\cos\theta_h$ for $0.03 \leq x_p \leq 0.8$. The statistical and systematic errors are combined quadratically.

x_p-interval	$(1/\sigma_h) \cdot \frac{d\sigma}{dx_p}$	$\cos\theta_h$-interval	$(1/\sigma_h) \cdot \frac{d\sigma}{d\cos\theta_h}$
0.03–0.06	0.82 ± 0.18	-1–(-0.5)	0.034 ± 0.008
0.06–0.10	0.38 ± 0.09	-0.5–0	0.031 ± 0.010
0.1–0.2	0.17 ± 0.05	0–0.5	0.033 ± 0.008
0.2–0.4	0.05 ± 0.02	0.5–1	0.033 ± 0.011
0.4–0.8	0.005 ± 0.003		

tion is compared with the predictions of the JETSET [15], HERWIG [17] and UCLA [18] models with the default parameters. The models grossly overestimate the $\Delta^{++}(1232)$ production rate, but reproduce reasonably well the shape of the x_p-spectrum apart from the region of large $x_p \geq 0.4$ for HERWIG, due to the overestimated contribution of the primary quark's

fragmentation into $\Delta^{++}(1232)$.

Extrapolation of the measured production rate (7) to the full x_p-range was performed by normalizing the JETSET, HERWIG and UCLA model expectations in the $0.03 \leq x_p \leq 0.8$ range to the measured $\Delta^{++}(1232)$ rate in this x_p-interval and by taking the average value of the $\Delta^{++}(1232)$ rate in the full x_p-range from the corresponding JETSET, HERWIG and UCLA predictions. This gave

$$< N(\Delta^{++}(1232) + \bar{\Delta}^{--}(1232)) >$$
$$= 0.079 \pm 0.009 \,(\text{stat}) \pm 0.009 \,(\text{syst})$$
$$\pm 0.007 \,(\text{extr}). \qquad (8)$$

The difference between the results of the extrapolation with these models was accounted for by the extrapolation error.

For the overall $\Delta^{++}(1232)$ multiplicity, the JETSET, HERWIG and UCLA models with default parameters predict respectively 0.189, 0.199 and 0.154, i.e. a factor of more than two higher than the value (8).

On the other hand, the value (8) agrees within errors with the estimate

$$< N(\Delta^{++}(1232) + \bar{\Delta}^{--}(1232)) > = 0.064 \pm 0.002$$

obtained in [19] from the exponential dependence on their mass squared of the spin/isospin weighted particle production rates in e^+e^- annihilations. The production rates of particles for one isospin projection (and with antibaryons not included) weighted with the factor $(2I_m + 1)/(2J + 1)$, where J is the particle spin and I the isospin (or modified isospin I_m for mesons, see [19]) are shown as a function of their masses squared in Fig. 6. The plot is taken from Ref. [19], but with the additional $\Delta^{++}(1232)$ data point included. A fit of the form $a\exp(-bM^2)$ to all the data except the pion (the straight line in Fig. 6) yields $a = 11.28 \pm 0.31$ and $b = 3.872 \pm 0.027$ $(\text{GeV}/c^2)^{-2}$ (as was also found in [19]), with $P(\chi^2) = 13\%$. Thus the production rates of all particles belonging to the SU(3) octet and decuplet baryons and to the nonets of pseudoscalar and vector mesons (apart from pions) as a function of their masses squared lie on one universal curve.

4. Summary

The $\Delta^{++}(1232)$ production rate is measured in hadronic Z decays at LEP. From this study the following conclusions can be drawn.

- The measured total $\Delta^{++}(1232)$ plus $\bar{\Delta}^{--}(1232)$ production rate of 0.079 $\pm$ 0.015 is less than half that predicted by the UCLA, JETSET and HERWIG models with default parameters, and also less than half compared to the value (0.22 $\pm$ 0.04 $\pm$ 0.04) recently measured by OPAL [13].
- The shape of the $\Delta^{++}(1232)$ x_p-spectrum is consistent with the shapes predicted by the JETSET, HERWIG and UCLA models, apart from the $x_p \geq 0.4$ region for HERWIG.
- The $\Delta^{++}(1232)$ production rate agrees well with the universal dependence of the production rates in e^+e^- annihilations of octet and decuplet baryons, and of nonets of pseudoscalar and vector mesons (apart from pions) on their masses squared which is described by a simple exponential $a\exp(-bM^2)$.

Acknowledgements

References

[1] OPAL Collab., R. Akers et al., Z. Phys. C 63 (1994) 181.
[2] DELPHI Collab., P. Abreu et al., Nucl. Phys. B 444 (1995) 3.
[3] ALEPH Collab., D. Buskulic et al., Z. Phys. C 66 (1995) 355.
[4] ALEPH Collab., D. Buskulic et al., Z. Phys. C 64 (1994) 361.
[5] DELPHI Collab., P. Abreu et al., Phys. Lett. B 275 (1992) 231.
[6] DELPHI Collab., P. Abreu et al., Strange Baryon Production in Z Hadronic Decays, CERN PPE/95-39 (1995).
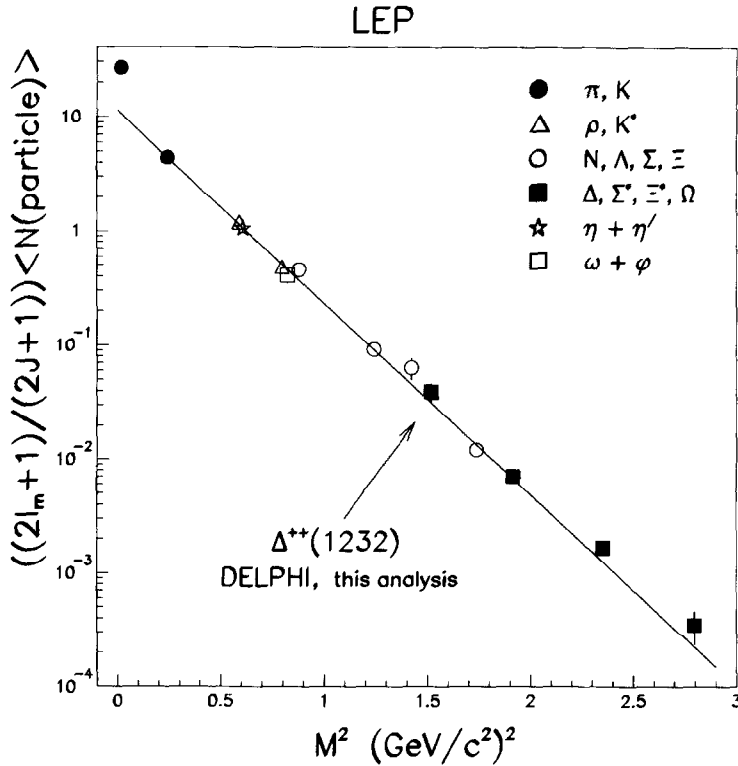
Fig. 6. Production rates of pseudoscalar and vector mesons, and octet and decuplet baryons at Z pole at LEP, weighted with the $(2I_m + 1)/(2J + 1)$ factor, as a function of particle masses squared. The production rates of particles measured by more than one experiment are averaged. The line shows the result of the fit to the form $a\exp(-bM^2)$.

[7] DELPHI Collab., Production of Σ^0 and Ω^- in Z Decays, paper eps0555 submitted to the "EPS-HEP 95" Conference, Brussels 1995 (DELPHI Note 95-96 PHYS 531).

[8] OPAL Collab., P.D. Acton et al., Phys. Lett. B 291 (1992) 503.

[9] OPAL Collab., Strange Baryon Production and Correlations in Hadronic Z decays, paper submitted to the 27th Int. Conf. on High Energy Physics, Glasgow, 1994.

[10] L3 Collab., M. Acciari et al., Phys. Lett. B 328 (1994) 223.

[11] ARGUS Collab., H. Albrecht et al., Phys. Lett. B 230 (1989) 169.

[12] TASSO Collab., M. Althoff et al., Z. Phys. C 26 (1984) 181.

[13] OPAL Collab., G. Alexander et al., Δ^{++} Production in Hadronic Z Decays, CERN-PPE/95-99 (1995).

[14] B. Andersson et al., Phys. Rep. 97 (1983) 31.

[15] T. Sjöstrand, Comp. Phys. Comm. 82 (1994) 74; CERN preprint CERN-TH.7112/93 (1993, revised August 1994).

[16] G. Marchesini and B.R. Webber, Nucl. Phys. B 238 (1984) 1.

[17] G. Marchesini et al., Comp. Phys. Comm. 67 (1992) 465.

[18] S.B. Chun and C.D. Buchanan, Phys. Lett. B 308 (1993) 153 and private communication from S.B. Chun.

[19] P.V. Chliapnikov and V.A. Uvarov, Phys. Lett. B 345 (1995) 313.

[20] DELPHI Collab., P. Aarnio et al., Nucl. Instr. Meth. A 303 (1991) 233.

[21] DELPHI Collab., Performance of the DELPHI Detector, paper eps0764 submitted to the "EPS-HEP 95" Conference, Brussels 1995 (DELPHI Note 95-112 PHYS 547).

[22] DELPHI Collab., P. Abreu et al., Z. Phys. C 65 (1995) 587.

[23] Particle Data Group, L. Montanet et al., Phys. Rev. D 50 (1994) 1173.